Current Biology 19, 260–265, February 10, 2009 ©2009 Elsevier Ltd All rights reserved DOI 10.1016/j.cub.2008.12.045

Report

Local Cortical Tension by Myosin II Guides 3D Endothelial Cell Branching

Robert S. Fischer,[1,*] Margaret Gardel,[2] Xuefei Ma,[3] Robert S. Adelstein,[3] and Clare M. Waterman[1,*]

[1]Laboratory of Cell and Tissue Morphodynamics
Cell Biology and Physiology Center
National Heart, Lung, and Blood Institute
National Institutes of Health
Bethesda, MD 20892
USA

[2]Department of Physics
University of Chicago
Chicago, IL 60637
USA

[3]Laboratory of Molecular Cardiology
Genetics and Developmental Biology Center
National Heart, Lung, and Blood Institute
National Institutes of Health
Bethesda, MD 20892
USA

Summary

A key feature of angiogenesis is directional control of endothelial cell (EC) morphogenesis and movement [1]. During angiogenic sprouting, endothelial "tip cells" directionally branch from existing vessels in response to biochemical cues such as VEGF or hypoxia and migrate and invade the surrounding extracellular matrix (ECM) in a process that requires ECM remodeling by matrix metalloproteases (MMPs) [2–4]. Tip EC branching is mediated by directional protrusion of subcellular pseudopodial branches [5, 6]. Here, we seek to understand how EC pseudopodial branching is locally regulated to directionally guide angiogenesis. We develop an in vitro 3D EC model system in which migrating ECs display branched pseudopodia morphodynamics similar to those in living zebrafish. Using this system, we find that ECM stiffness and ROCK-mediated myosin II activity inhibit EC pseudopodial branch initiation. Myosin II is dynamically localized to the EC cortex and is partially released under conditions that promote branching. Local depletion of cortical myosin II precedes branch initiation, and initiation can be induced by local inhibition of myosin II activity. Thus, local downregulation of myosin II cortical contraction allows pseudopodium initiation to mediate EC branching and hence guide directional migration and angiogenesis.

Introduction

In vivo, tip EC branching morphogenesis occurs in a compliant three-dimensional (3D) environment. Branching is regulated in part by actomyosin-mediated cellular sensing of environmental compliance and dimensionality. In "compliance mechanosensing," ECM stiffness and myosin II-mediated cell contractility are engaged in a feedback loop [7]. Stiffness is sensed by cell-ECM adhesions, which mediate RhoA activation of Rho-kinase (ROCK) to enhance adhesion and myosin II-mediated contractility [8, 9]. "Dimensionality mechanosensing" promotes differential responses to 2D and 3D ECM environments [10, 11]. For example, engagement of integrins on both dorsal and ventral surfaces of cells in 2D culture alters cytoskeletal organization, cell morphology, and cell migration compared to response to engagement of the same receptors only on the ventral surface [12, 13]. The notion that both cytomechanical and intracellular signaling is critical for angiogenesis is well established [14, 15]. Because directed tip EC migration requires ECM degradation by MMPs, local ECM loosening and remodeling near sites of adhesion may be critical to directing EC migration in vivo [3]. However, how cues of compliance and dimensionality feed back to regulate the actomyosin machinery to mediate EC branching morphogenesis and tip EC migration in physiological environments is unknown.

Results and Discussion

To facilitate our studies of tip EC migration in 3D, we first characterized dynamics of tip ECs in vivo to serve as a basis for development of a physiologically relevant model (Figures 1A–1C and [6]). We employed 4D microscopy to analyze the ECs in developing intersegmental vascular arches of zebrafish embryos stably expressing GFP driven by the endothelial-specific *fli-1* promoter (Figures 1A–1C). Similar to previous reports [5], tip ECs explored with long, thin protrusions that extended and retracted with characteristic rates (see Movies S1 and S4). EC protrusions displayed branches with small lamellipodia-like structures and bulges along their lengths and at their tips (see Figures 1B and 1C). Because these protrusions are not yet characterized according to their content of F-actin regulatory components, we will refer to them generically as "pseudopodia."

For our in vitro EC model, we used mouse aortic explants embedded within a 3D collagen fibrillar matrix. ECs migrated from explants singly as well as collectively in multicellular tube structures (Figures 1D–1G), in both cases retaining endothelial differentiation status (Figure S1 available online). Both single ECs and ECs at the tips of multicellular tubes form branched pseudopodia (Figures 1E and 1F) similar in morphology to pseudopodia on tip ECs in vivo (Figures 1B and 1C). Time-lapse imaging revealed that both single and tip mouse ECs on multicellular tubes approximated zebrafish tip EC dynamics in vivo, by moving through the collagen matrix with similar branched pseudopodia with small lamellipodia on their sides and ends (Figure 1G, Movies S3 and S4, and Figures S2A and S2B). Importantly, the protrusion and retraction rates (Figures 1G and 1H), length range (~10–78 μm in vivo, ~10–95 μm in vitro), and temporal persistence (11.3 + 7.8 min in vitro; 14.0 + 4.3 min in vivo) of pseudopodia on both single and tip mouse ECs in collagen gels were similar to those of pseudopodia on zebrafish tip ECs (Movie S4). Thus, although the overall movement of single and tip ECs differs because of cell-cell junctions, single mouse EC pseudopodial protrusion behavior is similar to that of tip ECs in vitro and in vivo [16].

*Correspondence: fischerr2@mail.nih.gov (R.S.F.), watermancm@nhlbi.nih.gov (C.M.W.)

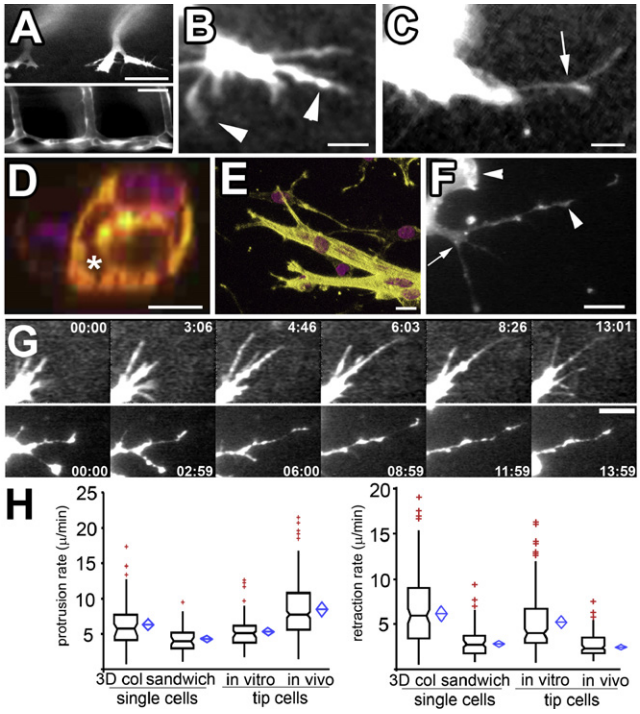

Figure 1. ECs in Vivo and in 3D Collagen Matrices in Vitro Exhibit Similar Pseudopodial Morphology and Dynamics

(A–C) Confocal images of living ECs expressing GFP during zebrafish embryonic angiogenesis (see Movie S1). Intersegmental vessels ([A], bottom), 7 days after fertilization, form from branched tip ECs ([A], top, 24 hr after fertilization). (B) and (C) show higher-magnification views of living tip ECs (Movies S1 and S3). Arrows indicate branch points along pseudopodia; arrowheads indicate tip and side lamellipodia-like bulges. Scale bars in (A) represent 40 μm and 80 μm (top and bottom, respectively). Scale bars in (B) and (C) represent 21 μm.

(D) Cross-section of mouse endothelial tube structure formed in 3D collagen matrices: violet, DAPI-stained nuclei; yellow, phalloidin-stained F-actin; asterisk, lumen formed between cells. The scale bar represents 10 μm.

(E) Three-dimensional reconstructions of mouse endothelial tube tips formed in 3D collagen. The scale bar represents 12 μm.

(F) Confocal image of living mouse aortic ECs expressing GFP-β-actin in a 3D collagen matrix. Branch points (indicated by an arrow) and lamellipodia (indicated by arrowheads) and bulges along pseudopodia are highlighted. The scale bar represents 31 μm.

(G) Images from time-lapse confocal series showing protrusion dynamics of zebrafish tip ECs in vivo (top) and in mouse ECs in 3D collagen matrices in vitro (bottom); time in min:s is shown. The scale bar represents 12 μm.

(H) Protrusion (left graph) and retraction rates (right graph) of pseudopodia of single ECs or tube tip cells in 3D collagen matrices ("3D col"), 450 kPa collagen/PA/glass sandwich gels ("sandwich"), and zebrafish tip ECs in vivo. In this and subsequent figures, boxes represent median and center quartiles, blue diamonds represent 95% confidence limit means, and red plusses represent outliers of >1.5 and <3.0 interquartile range. For statistical analysis, see Table S1.

For some experiments, we desired to control the compliance of the in vitro 3D environment. To affect compliance without altering 3D collagen access, we covalently coupled 3D collagen matrices to polyacrylamide (PA) gels of defined elastic modulus (Figure 2) and affixed these to microscope coverslips, to make collagen/PA/glass "sandwich gels." ECs in the collagen at the PA-collagen interface (Figure 2A) engage on their ventral-surface collagen covalently coupled to PA of defined stiffness, but also engage dorsal collagen in the 3D matrix. Because the collagen matrices were softer than the underlying PA (see Supplemental Experimental Procedures), the maximum stiffness encountered by the cells was collagen coupled to the PA. In 0.45 kPa collagen/PA/glass sandwich gels, ECs displayed an elongated, spindle-like morphology with extended pseudopodial branches. Quantification of their pseudopodial protrusion and retraction behavior revealed dynamics similar to tip ECs in zebrafish in vivo and mouse ECs in 3D collagen matrices (Figures 1E, 1F, and 2B; also compare Movies S3 and S6, right). In conclusion, single mouse ECs in both collagen matrices and collagen/PA/glass sandwich gels provide a physiologically relevant 3D model system amenable to high-resolution microscopy to study EC protrusion and branching.

Pseudopodial Branching Is Initiated by Lamellipodial Protrusion and Inhibited by ECM Stiffness and ROCK-Mediated Myosin II Activity

We first characterized pseudopodial branch initiation and its contribution to directional migration. During migration, which was generally radially away from the aortic explant, ECs exhibited localized sites of lamellipodial activity along their branches and cell bodies. Some lamellipodia extended away from the EC to form new pseudopodial branches (Figures S2A; Movies S3 and S5). Most pseudopodia rapidly retracted back into the cell body, but a few persisted. The persistent branches that generated sufficient adhesion and force on the ECM (indicated by collagen deformation; Figure S2B and Movie S5) to pull the cell body consequently changed the direction of cell migration. Thus, EC branches are initiated from lamellipodia, and persistent branches mediate EC pathfinding.

To determine the role of ECM compliance in regulating branching, we examined ECs in collagen/PA/glass sandwich gels. ECs in soft sandwich gels (0.45 kPa PA) branched and migrated similarly to ECs in 3D collagen matrices (Figure 2B; Movie S6, right, and Movie S7, top). Stiffening the PA in the sandwich gel (14 kPa) induced spindle-shaped ECs with significantly fewer branches (Figure 2D) but did not alter overall radial migration from the explant (Figure 2E; Movie S6, left, and Movie S7, bottom). Limiting collagen access to 2D by replating ECs on top of a 2D layer of collagen covalently coupled to soft PA (0.45 kPa) induced cell aggregation, with some single cells exhibiting small lamellae and a few branched extensions (Figure 2H; Movie S8). Stiffening the PA in this 2D system (14 kPa) caused ECs to spread with large, unbranched lamellae, similar to ECs cultured on plastic or glass (Figure 2I; see also Movie S8). Quantification of EC branch number showed that, for the same compliance, 3D collagen engagement enhanced cell branching compared to 2D (Figure 2G). Therefore, increased ECM stiffness inhibits EC branching morphogenesis, and three dimensionality is synergistic with compliance in promoting branching.

To determine whether inhibition of EC branching by 3D ECM stiffness is linked to myosin II activity, we perturbed EC myosin II function in either stiff (14 kPa) or soft (0.45 kPa) collagen/PA/glass sandwich gels and examined branch formation. Myosin II ATPase inhibition with 30 μM blebbistatin significantly increased EC branching in both soft (Figure 2C) and stiff (Figure 2F) sandwich gels. The response of ECs to both decreased ECM stiffness and inhibition of myosin II was synergistic as compared with either treatment alone (Figure 2D), suggesting that softer ECM may enhance EC sensitivity to decreased myosin II activity.

Myosin II can be regulated by phosphorylation of its light chains by myosin light chain kinase (MLCK) or ROCK [17, 18]. To determine which pathway mediated myosin II

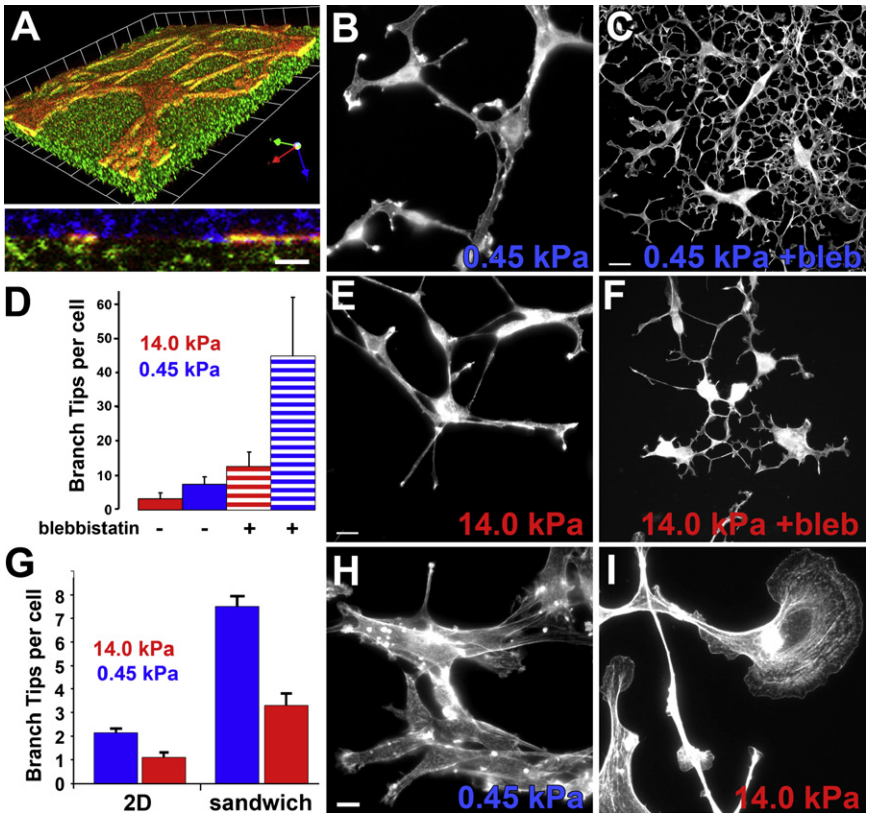

Figure 2. ECM Stiffness Is Synergistic with ROCK-Mediated Myosin II Activity in Inhibiting EC Branching

(A–E) Mouse aortic ECs grown in collagen/PA/glass "sandwich gels" (see text, Supplemental Experimental Procedures) with F-actin stained with BODIPY-phallacidin. (A) shows a 3D reconstruction of confocal image Z series of mouse aortic cells expressing GFP-actin (red) in a collagen/PA/glass sandwich gel. The top image shows a skewed view; grid unit = 9.8 μm, the bottom image shows a X-Z view. Cell is at the interface between the collagen covalently bound to the PA (embedded with fluorescent microspheres, green) and surrounding 3D collagen (immunolabeled, blue). The scale bar in the bottom panel of (A) represents 12 μm. The error bar in (D) indicate SD.

(B, C, E, and F) Maximum intensity projections of confocal image z series. ECs in soft ([B] and [C], 0.45 kPa) or stiff ([E] and [F], 14 kPa) collagen/PA/glass sandwich gels, with ([C] and [F], 30 μM) or without (B and E) blebbistatin treatment.

(D) shows quantification of branches per cell for ECs in collagen/PA/glass sandwich gels of the stiffness shown, with or without 30 μM blebbistatin treatment. Scale bars in (C) and (F) represent 12 μm. Scale bars in (B) and (E) represent 9 μm.

(G) Quantification of branch tips per cell on 2D collagen/PA substrates versus in collagen/PA/glass sandwich gels. Error bars in (G) indicate SEM.

(H and I) Mouse ECs stained with BODIPY-phallacidin on soft ([H], 0.45 kPa) or stiff ([I], 14 kPa) PA gels covalently coupled with a 2D layer of collagen. For statistical analysis, see Table S1.

regulation of EC branching, we used pharmacological inhibitors on ECs in 3D collagen matrices. As observed in collagen/PA/glass sandwich gels, inhibition of myosin II ATPase with blebbistatin in 3D collagen increased EC branching as compared to controls (Figure S3; Movie S9), whereas the inactive +/+ enantiomer of blebbistatin had no effect (Figure S3). Inhibition of Rho GTPase by cell permeable C3 exoenzyme or ROCK by either 10 μM Y-27632, or 2 μM H-1152 (Figure S3) [19] also increased EC branching. ROCK-inhibited cells maintained bipolar morphology (Figure S3) and continued to move, but they were unable to define a leading versus trailing end (Movie S9). Inhibition of MLCK with 1-2 μM ML-7 did not enhance EC branching, but promoted blebbing (Figure S3).

Pseudopodium initiation, protrusion, and retraction may all contribute to EC steady-state branch morphology. To identify which of these processes are regulated by myosin II, we perturbed myosin II function in ECs in collagen matrices and quantified parameters of pseudopodial branch dynamics (Figures 3A–3C). Compared to controls, either blebbistatin or Y-27632 had no significant effect on protrusion rates but decreased pseudopodia retraction rates, (Figures 3A and 3B). Y-27632 also increased the frequency of pseudopodium initiation (defined as extensions $\geq$5 μm from the cell body) (Figure 3C). Similarly, pseudopodium initiation was increased in ECs in soft compared to stiff collagen/PA/glass sandwich gels (Figure 3C). The complex shape of blebbistatin-treated ECs precluded reliable quantification of branch initiation. However, together these data show that contractility via Rho- and ROCK-mediated myosin II activity and/or ECM stiffness inhibits EC branching by both blocking pseudopodium initiation and retracting branches after their successful initiation.

Regulation of Branch Initiation via Myosin II Controls Directed EC Migration and ECM Invasion

Given that ECs follow the direction of the most stable branch, increased branching could affect EC invasion into 3D ECM and/or migration directional persistence. In control collagen matrices, ECs invaded extensively into the ECM (Figure 3G and Movie S9), whereas inhibition of myosin II (Figure 3G) or ROCK (not shown) markedly reduced this invasion distance. Quantification showed that reduced invasion was due to decreases in both EC speed and directional persistence (Figures 3D and 3E). With blebbistatin, directional persistence and speed were affected by both a lack of EC polarization due to superfluous pseudopodia as well as decreased tail retraction, whereas ROCK inhibition had a stronger effect on polarization than speed (Movie S9 and Figure 3D). This contrasts cells in 2D culture, in which myosin II inhibition decreases directional persistence, but enhances cell speed [20]. Additionally, ECs in soft (0.45 kPa) collagen/PA/glass sandwich gels showed decreased directional persistence relative to those in stiffer (14 kPa) sandwich gels (Figures 3E and 3F). Thus, Rho- and ROCK-mediated myosin II contractility or ECM stiffness promotes 3D ECM invasion by inhibiting EC branching to encourage directional persistence and enhance migration speed.

Myosin II Activity and Stability within the F-Actin Cortex Regulates EC Branching

To understand how myosin II inhibits pseudopodial branch formation, we examined the 3D localization of myosin IIs in ECs in 3D collagen matrices from transgenic mice in which endogenous myosin IIB was replaced by GFP-myosin IIB. F-actin, GFP-myosin IIB, and myosin IIA (by

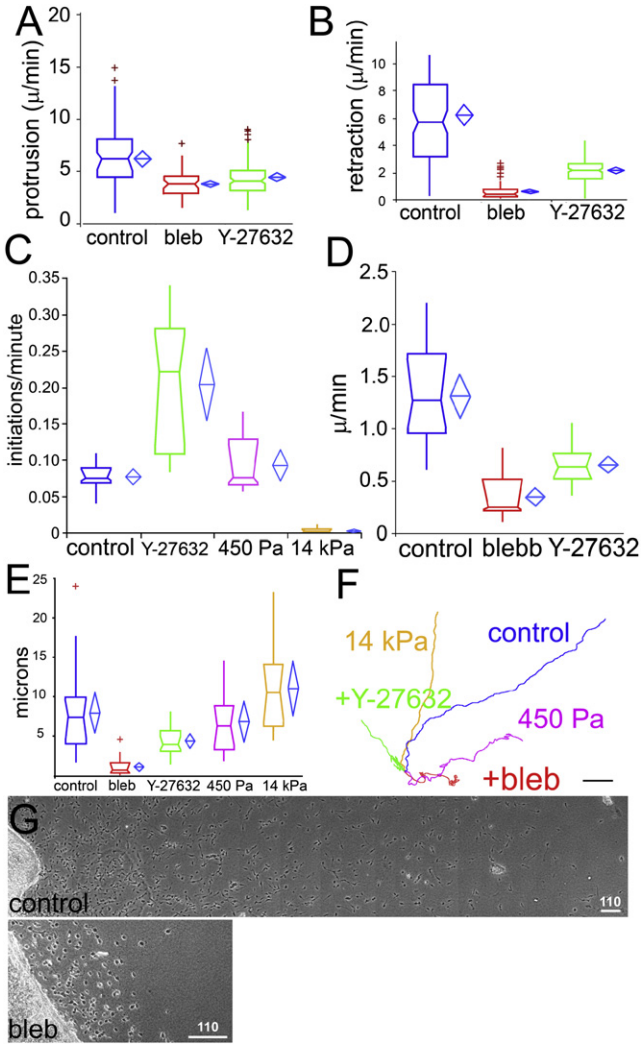

Figure 3. ROCK-Mediated Myosin II Activity Regulates Pseudopodial Dynamics and EC Migration and Invasion in 3D Collagen Gels

Parameters were measured from phase-contrast time-lapse movies of mouse aortic ECs in 3D collagen matrices (untreated [control] or treated with 30 μM blebbistatin [bleb] or 10 μM Y-27632) or in collagen/PA/glass sandwich gels of the indicated elastic moduli (450 Pa, 14kPa). Protrusion (A) and retraction (B) rates of individual pseudopodia are shown. (C) shows the pseudopod initiation frequency per cell per minute (see Supplemental Experimental Procedures). EC migration speed (D) and migration directional persistence distance (E) are measured as described [20]. (F) shows an example of 189-min-long EC migration path traces. For statistical analysis, see Table S1. Boxes represent median and center quartiles, blue diamonds represent 95% confidence limit means, and red plusses represent outliers of >1.5 and <3.0 interquartile range. (G) shows montages of images of mouse aortic cultures in 3D collagen matrices after 2 days' treatment with either vehicle (control) or 30 μM blebbistatin (bleb). The scale bars in (F) and (G) represent 10 and 110 μm, respectively.

immunofluorescence) all colocalized to the cortex, and both myosin II isoforms additionally formed a fibrillar cytoplasmic pool (Figures 4A–4C and Figures S2A–S2D). Glancing optical sections of the cortex showed that myosin IIB and F-actin formed longitudinal bundles reminiscent of actomyosin bundles or stress fibers in 2D cultures [21] (Figure 4 and Movies S10 and S11). ROCK-mediated myosin II contractility was required for forming or maintaining the bundles because Y-27632 or blebbistatin abolished them (Figures 4E–4G, Movie S12, and Figures S4E–S4H). Time-lapse imaging showed that myosin IIB puncta formed and then coalesced into a web-like array behind the advancing tip of newly protruding pseudopodia (Movie S11; Figures 4D and 4H), similar to punctae in the lamella of cells in 2D culture [22] (Movie S11). Thus, myosin II acts at the EC cortex, where it is dynamically colocalized with F-actin.

To determine whether myosin II activity is regulated under conditions that modulate EC branching, we quantified Ser19 phosphomyosin II light chain by immunofluorescence of ECs in either soft (300 Pa) or stiff (14.5 kPa) collagen/PA/glass sandwich gels (Figure 4I). Ratio imaging with F-actin staining revealed a higher phosphomyosin II light chain:F-actin level in stiffer as compared to softer ECMs (Figure S6A). In addition to regulation by light-chain phosphorylation, myosin II activity could be modulated by the stability of its cortical binding. To test this, we analyzed fluorescence recovery after photobleaching (FRAP) of GFP-myosin IIB at the EC cortex in soft (300 Pa) versus stiff (14.5 kPa) collagen/PA/glass sandwich gels (Figures 4J and 4K; Figure S6B). This revealed that in stiffer sandwich gels, a significantly larger fraction of GFP-myosin IIB in ECs was stably associated with the cortex as compared to that in ECs in softer environments (Figure 4J). Although fluorescence recovery of the mobile fraction of cortical GFP-myosin IIB was faster in ECs in stiff compared to soft ECMs, the difference was not significant (Figure 4K), suggesting that the mobile fraction probably recovers via the same mechanism in the two conditions. In both soft and stiff ECMs, cytosolic GFP-myosin IIB fluorescence recovered rapidly and completely (data not shown). Thus, ECM stiffness may inhibit pseudopodial branching by both promoting myosin II's light-chain phosphorylation and stable association with the EC cortex.

We next hypothesized that local downregulation of cortical myosin II may allow pseudopodial branch initiation. In support of this, time-lapse images of GFP-myosin IIB showed that local alterations in cortical GFP-myosin IIB density preceded pseudopodial initiation. Prior to branch initiation, myosin IIB localized relatively uniformly along the cortex. Local thinning of the myosin IIB cortical fluorescence caused gaps in localization flanked by brighter puncta, followed by lamellipodial protrusions extending from the gaps, and these lamellipodia went on to form persistent pseudopodial branches. Thus, local depletion of cortical myosin IIB precedes lamellipodium-mediated branch initiation.

To determine whether local inhibition of cortical myosin II is sufficient to induce pseudopodial branch formation, we applied blebbistatin locally to unbranched regions of ECs in 3D collagen matrices using a microinjection pipette. Remarkably, this caused lamellipodial protrusion and pseudopodium extension near the point of application and toward the pipette tip in 9/20 samples (Figure 4M; Movie S14). Branches were never induced on the cell side opposite the local application, nor with vehicle alone (0/20 samples, $p = 3.3 \times 10^{-4}$; F/Fcrit = 3.79). Thus, local inhibition of cortical myosin II function is sufficient to induce EC branching.

We propose a model of myosin II regulation of directed EC migration in a heterogenous, physiological 3D ECM environment (Figure S7). In vivo, local cues such as VEGF or hypoxia are probably transduced by tip ECs into signals that induce transient lamellipodial protrusions. Myosin II generates tension in the EC cortex to retract most protrusions. In regions where local ECM loosening (e.g., by MMP action) is encountered, contractility is locally downregulated by

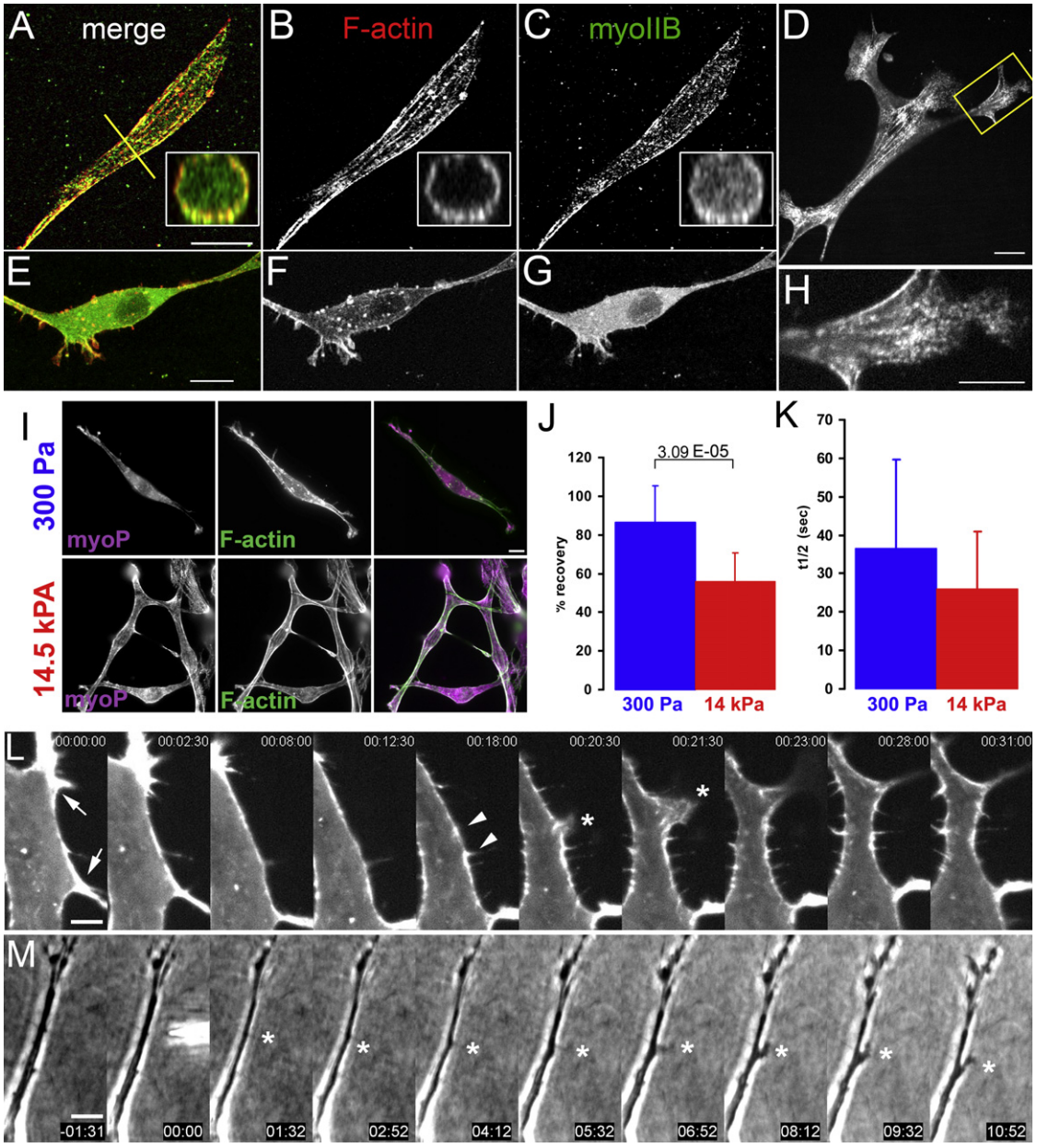

Figure 4. Myosin II Activity and Stability within the F-Actin Cortex Regulates EC Branching

(A–D) Maximal projections of 3D reconstructions of laser-scanning confocal Z image series of GFP myosin IIB (C and G), and bodipy phallacidin staining of F-actin (B and F) in mouse ECs in 3D collagen matrices. Insets show X-Z cross-sections taken along the yellow lines in (A). The scale bar in (A) represents 14 μm. Error bars in (B) and (C) represent SD.

(E–G) Similar EC to in (A)–(C) but treated with 10uM Y27632. The scale bar in (E) represents 10 μm.

(D and H) Single spinning-disk confocal image of a living mouse EC expressing GFP-myosin IIB. (H) shows a magnification of the area boxed in (D). The scale bars in (D) and (H) represent 4 μm.

(I) Localization of serine-19 phosphorylated myosin light chain 2 ([myoP] by immunostaining) and F-actin (by fluorescent phalloidin) in mouse ECs in soft (300 Pa, top row) versus stiff (14.5kPa, bottom row) collagen/PA/glass sandwich gels. The scale bar represents 12 μm.

(J and K) Analysis of cortical GFP-myosin IIB FRAP in mouse aortic ECs in collagen/PA/glass sandwich gels of the noted elastic moduli; error bars represent the standard deviation. (J) shows the mean percent fluorescence recovery to steady state. (K) shows the mean half-time of fluorescence recovery.

(L) Montage of time-lapse confocal images of GFP-myosin IIB during pseudopodial branch initiation in mouse aortic ECs in 3D collagen gels; time is shown in min:s. Cortical GFP-myosin IIB intensity locally depletes (between arrows, times 00:00–12:30), collecting in two puncta (indicated by arrowheads). Asterisks mark lamellipodial protrusion between former puncta, which extends into a pseudopodial branch (times 23:00–31:00). The scale bar represents 3.3 μm.

(M) Time-lapse phase-contrast images of local application of 40 μM blebbistatin to an EC in a collagen matrix. Time shown is relative to drug application in min:s; microneedle containing drug is visible at time 00:00. Asterisks mark application site. The scale bar represents 10 μm. For statistical analysis, see Table S1.

mechanosensory feedback that reduces light-chain phosphorylation and releases cortical myosin II. Local myosin II downregulation allows lamellipodia to initiate a branch by "escaping" retraction by cortical tension. For the branch to change EC migration direction, the exploratory lamellipodium at its tip must encounter and adhere to more distal ECM stiff

enough to allow re-establishment of actomyosin contractility to pull the cell in the new direction. Thus, in uniformly soft ECMs, ECs initiate many branches, and fewer branches are successful in stably changing direction, thereby decreasing migration polarity and directional persistence. Conversely, in stiffer ECM, fewer pseudopodia branches escape myosin II cortical tension, thereby focusing migration along collagen fibrils in the existing branch direction. Our data provide a mechanistic framework to understand long-held ideas regarding the role of the Rho pathway, myosin II contractility and ECM mechanics in vascular development in normal and tumor tissue, and endothelial cell migration both in vivo and in vitro [14] [23] [24], via regulation of myosin II activity and dynamics at the cell cortex.

Experimental Procedures

Methods have been described in general in the text. For experimental details, please see Supplemental Experimental Procedures.

Supplemental Data

Supplemental Data include 6 figures, 14 movies, and a table of statistical comparisons, as well as Supplemental Experimental Procedures, and can be found with this article online at http://www.current-biology.com/supplemental/S0960-9822(09)00538-7.

Acknowledgments

We thank Roberta Nowak and Velia Fowler (Scripps Research Institute, La Jolla, CA, USA) for maintaining GFP-actin mice, Konstantin Stoletov and Richard Klemke (UCSD, San Diego, CA, USA) for *fli1-gfp* zebrafish embryos, and Gaudenz Danuser (Scripps) for technical advice and constructive discussion. We would also like to thank Mary Anne Conti for critical reading of the manuscript. This work was supported by the Intramural Research Program of the NIH/NHLBI.

Received: July 7, 2008
Revised: December 19, 2008
Accepted: December 22, 2008
Published online: January 29, 2009

References

1. Carmeliet, P. (2000). Mechanisms of angiogenesis and arteriogenesis. Nat. Med. *6*, 389–395.
2. Gerhardt, H., and Betsholtz, C. (2005). How do endothelial cells orientate? EXS, 3–15.
3. Heissig, B., Hattori, K., Friedrich, M., Rafii, S., and Werb, Z. (2003). Angiogenesis: Vascular remodeling of the extracellular matrix involves metalloproteinases. Curr. Opin. Hematol. *10*, 136–141.
4. Hotary, K.B., Yana, I., Sabeh, F., Li, X.Y., Holmbeck, K., Birkedal-Hansen, H., Allen, E.D., Hiraoka, N., and Weiss, S.J. (2002). Matrix metalloproteinases (MMPs) regulate fibrin-invasive activity via MT1-MMP-dependent and -independent processes. J. Exp. Med. *195*, 295–308.
5. Lawson, N.D., and Weinstein, B.M. (2002). In vivo imaging of embryonic vascular development using transgenic zebrafish. Dev. Biol. *248*, 307–318.
6. Gerhardt, H., Golding, M., Fruttiger, M., Ruhrberg, C., Lundkvist, A., Abramsson, A., Jeltsch, M., Mitchell, C., Alitalo, K., Shima, D., et al. (2003). VEGF guides angiogenic sprouting utilizing endothelial tip cell filopodia. J. Cell Biol. *161*, 1163–1177.
7. Peyton, S.R., Kim, P.D., Ghajar, C.M., Seliktar, D., and Putnam, A.J. (2008). The effects of matrix stiffness and RhoA on the phenotypic plasticity of smooth muscle cells in a 3-D biosynthetic hydrogel system. Biomaterials *29*, 2597–2607.
8. Beningo, K.A., Hamao, K., Dembo, M., Wang, Y.L., and Hosoya, H. (2006). Traction forces of fibroblasts are regulated by the Rho-dependent kinase but not by the myosin light chain kinase. Arch. Biochem. Biophys. *456*, 224–231.
9. Olson, M.F. (2004). Contraction reaction: Mechanical regulation of Rho GTPase. Trends Cell Biol. *14*, 111–114.
10. Frey, M.T., Tsai, I.Y., Russell, T.P., Hanks, S.K., and Wang, Y.L. (2006). Cellular responses to substrate topography: Role of myosin II and focal adhesion kinase. Biophys. J. *90*, 3774–3782.
11. Discher, D.E., Janmey, P., and Wang, Y.L. (2005). Tissue cells feel and respond to the stiffness of their substrate. Science *310*, 1139–1143.
12. Beningo, K.A., Dembo, M., and Wang, Y.L. (2004). Responses of fibroblasts to anchorage of dorsal extracellular matrix receptors. Proc. Natl. Acad. Sci. USA *101*, 18024–18029.
13. Even-Ram, S., and Yamada, K.M. (2005). Cell migration in 3D matrix. Curr. Opin. Cell Biol. *17*, 524–532.
14. Mammoto, A., Mammoto, T., and Ingber, D.E. (2008). Rho signaling and mechanical control of vascular development. Curr. Opin. Hematol. *15*, 228–234.
15. Ingber, D.E. (2002). Mechanical signaling and the cellular response to extracellular matrix in angiogenesis and cardiovascular physiology. Circ. Res. *91*, 877–887.
16. Friedl, P. (2004). Prespecification and plasticity: Shifting mechanisms of cell migration. Curr. Opin. Cell Biol. *16*, 14–23.
17. Conti, M.A., and Adelstein, R.S. (2008). Nonmuscle myosin II moves in new directions. J. Cell Sci. *121*, 11–18.
18. Clark, K., Langeslag, M., Figdor, C.G., and van Leeuwen, F.N. (2007). Myosin II and mechanotransduction: A balancing act. Trends Cell Biol. *17*, 178–186.
19. Ikenoya, M., Hidaka, H., Hosoya, T., Suzuki, M., Yamamoto, N., and Sasaki, Y. (2002). Inhibition of rho-kinase-induced myristoylated alanine-rich C kinase substrate (MARCKS) phosphorylation in human neuronal cells by H-1152, a novel and specific Rho-kinase inhibitor. J. Neurochem. *81*, 9–16.
20. Lo, C.M., Buxton, D.B., Chua, G.C., Dembo, M., Adelstein, R.S., and Wang, Y.L. (2004). Nonmuscle myosin IIb is involved in the guidance of fibroblast migration. Mol. Biol. Cell *15*, 982–989.
21. Kolega, J. (1997). Asymmetry in the distribution of free versus cytoskeletal myosin II in locomoting microcapillary endothelial cells. Exp. Cell Res. *231*, 66–82.
22. Verkhovsky, A.B., Svitkina, T.M., and Borisy, G.G. (1995). Myosin II filament assemblies in the active lamella of fibroblasts: Their morphogenesis and role in the formation of actin filament bundles. J. Cell Biol. *131*, 989–1002.
23. Mavria, G., Vercoulen, Y., Yeo, M., Paterson, H., Karasarides, M., Marais, R., Bird, D., and Marshall, C.J. (2006). ERK-MAPK signaling opposes Rho-kinase to promote endothelial cell survival and sprouting during angiogenesis. Cancer Cell *9*, 33–44.
24. Matsumoto, T., Yung, Y.C., Fischbach, C., Kong, H.J., Nakaoka, R., and Mooney, D.J. (2007). Mechanical strain regulates endothelial cell patterning in vitro. Tissue Eng. *13*, 207–217.